Supplementary Information

On the Peculiar EPR Spectra of P1 Centers at High (12-20 T) Magnetic Fields

Orit Nir-Arad[1], Eyal Laster[1], Mais Daksi[1], Nurit Manukovsky[1], and Ilia Kaminker[*1].

[1]*School of Chemistry, Faculty of Exact Sciences, Tel Aviv University, Tel Aviv 6997801, Israel.*

** - Corresponding Author (iliakam@tauex.tau.ac.il)*

Energy levels for a single P1 center

Figure S1 shows the energy levels for a P1 center at (a,b) 13.8 T and (c) 6.9 T as a function of θ. As mentioned in the main text, at 13.8 T there is a shift from strong to weak coupling regimes as θ increases, and the cancellation condition is strictly fulfilled for $\theta = 70.5°$. While the shift between the different coupling regimes is very apparent in transition probabilities, shown in Figure 3 in the main text, the exact cancellation condition is not apparent from the energy level diagram for $Q = 0\ MHz$ (Figure S1a), where the change in energy of levels $|4\rangle$ and $|6\rangle$ is symmetric, and the plot is dominated by changes in A_{eff}. For $Q = -3.973\ MHz$ (Figure S1b), changes in A_{eff} still dominate the energy levels diagram, with the non-zero quadrupolar interaction responsible for the asymmetry in the energy levels' dependence on θ. When the energy levels are plotted for 6.9 T with $Q = -3.973\ MHz$ (Figure S1c), the changes in A_{eff} are still the main effect, but the relative change is much smaller than that observed at 13.8 T. The 13.8 T energy level diagram is surprising since an anticrossing is expected upon transition from strong to weak coupling. It appears that the reason is that even for the P1 centers with $\theta = 0°$, which are the furthest from the exact cancellation condition, the spin system is still close enough to it, and thus the shift between different regimes is not apparent. This is supported by the fact that the energy levels in the $m_S = +½$ manifold are much closer to one another with the energy separation $\left(Energy(|6\rangle) - Energy(|4\rangle)\right)/_{h \cdot \nu_{14N}}$ ranging from 0.1 to 0.7 at 13.8 compared to 1.8 to 3.4 at 7 T, for θ between $0°$ and $90°$.

Simulated EPR spectra of P1 centers in a single-crystal diamond

As explained in the main text, up to four symmetry related sites can be observed due to the symmetry of the diamond crystal. Figure S2a shows such a case with the diamond crystal oriented with the B_0 field normal to the (100) plane where all four P1 defects have the same $\theta = \mathrm{atan}\left(\sqrt{2}\right) \approx 54.73°$, resulting in a single triplet observed in EPR. For a crystal orientated in Orientation A $(0°, 58.2°, 0°)$, Figure S2c, there are two pairs of sites with equal intensity, each contributing a triplet with the central $(m_S = 0)$ line of both sites coinciding. For a crystal orientated in Orientation B $(-85.8°, -12.6°, 24.8°)$, Figure S2e, all four sites are resolved, each consisting of a triplet. In EPR spectra at 13.8 T, each site can contribute up to nine lines, their relative intensities depending on the angle of the site which determines how close each site is to the cancellation condition. When the (100) plain is perpendicular to the magnetic field (Figure S2b), all four sites are degenerate, and there are nine lines visible in the spectrum, as θ deviates by ~ $16°$ from

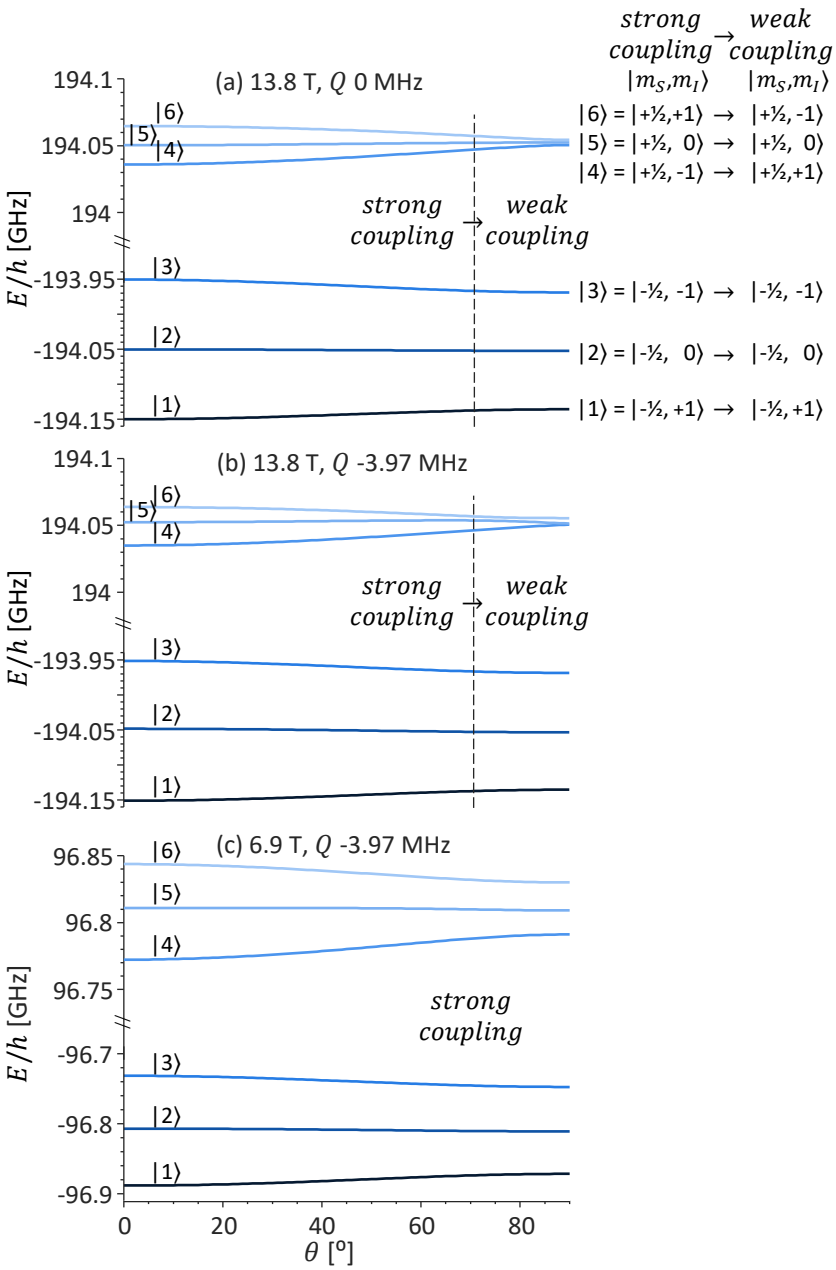

Figure S1: Energy levels diagram of a single P1 center spin system at B_0 = 13.8 T and (a) Q = 0 MHz and (b) Q = -3.97 MHz, and at (c) B_0 = 6.9 T and Q = -3.97 MHz.

meeting the cancellation condition. For the crystal at Orientation A (Figure S2d) site I ($\theta = 37.35°$) is in the strong coupling regime, with the spectrum composed of nine lines, and site II ($\theta = 79.27°$) is in the weak coupling regime, with only seven visible lines. Site II is closer to the cancellation condition, with θ deviating by ~ 9°, and we expect nine lines to be visible in the spectrum, but due to the overlap, only seven lines are resolved. Figure 6d in the main text shows the contribution of each transition to the simulated spectrum of each site for a diamond crystal at Orientation A at 13.8 T. Lastly, for a diamond crystal at Orientation B (Figure S2f), where all four sites are magnetically distinct, the spectrum is composed of a total of 35 lines, with all nine lines being resolved for three out of the four sites.

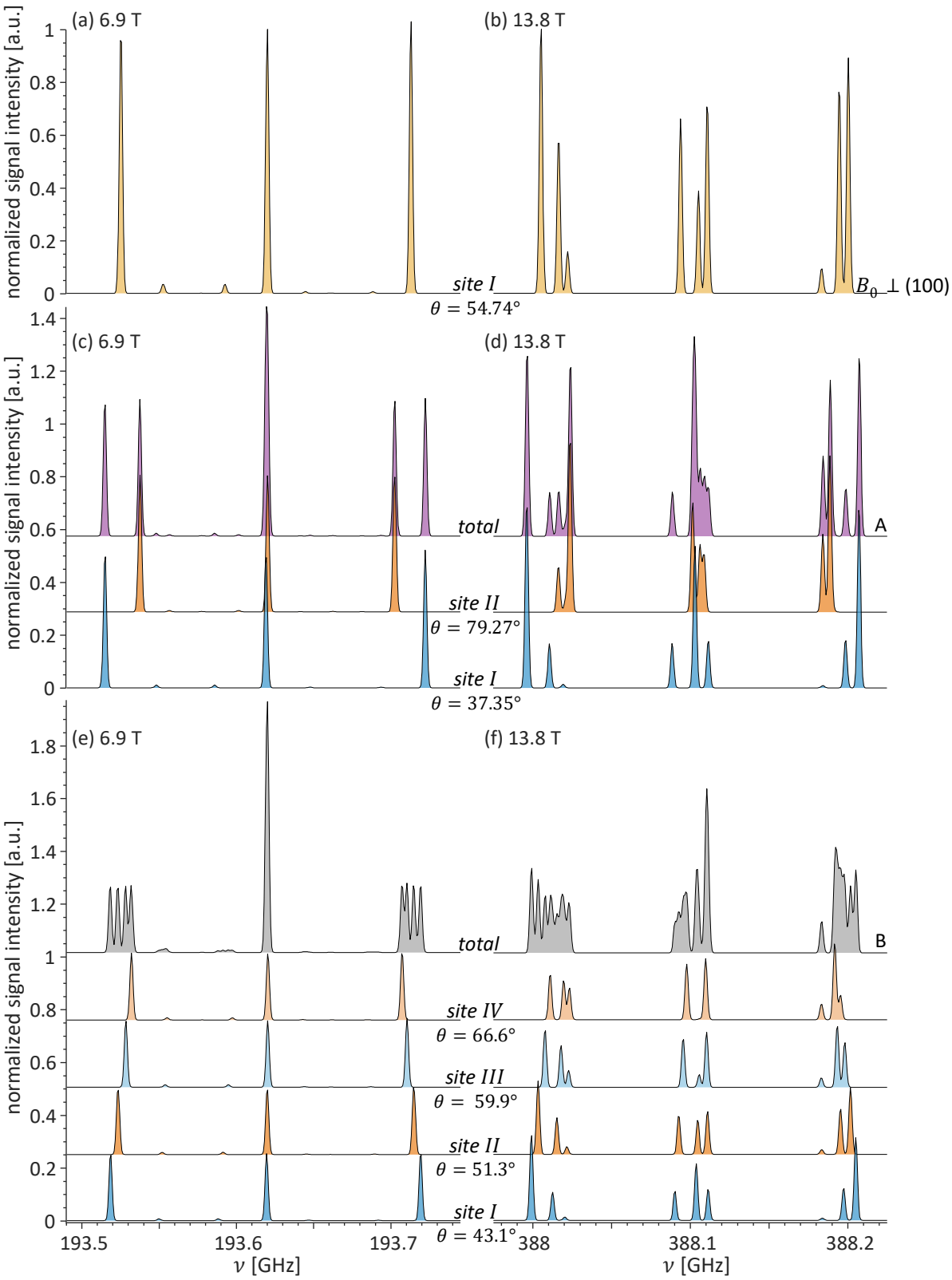

Figure S2: Decomposition into contributions from the individual sites of the simulated EPR spectra of P1 centers in a single crystal diamond vs crystal orientation, shown in Figure 4. (a,b) B_0 normal to (100) plane, (c,d) crystal at Orientation A, and (e,f) crystal at Orientation B for (a,c,e) 6.9 T and (b,d,f) 13.8 T.

Contribution of isolated P1 centers, P1 pairs, and P1 clusters populations to the experimental EPR spectra

For all diamond samples used in this work, three distinct populations of P1 centers are visible in the experimental pulsed EPR spectra. The first, and well documented population, is that of the isolated P1 centers, which exhibit one well-resolved triplet per crystallographic site. The second is of P1 centers pairs with strong dipolar coupling with each other. These are accounted for in the simulation by using identical parameters to the isolated P1 with increased linewidth. The resulting spectrum consists of three broad lines and looks identical for all the crystallographic sites. The last population consists of P1 centers clusters with strong exchange coupling with each other, which exhibit a broad spectrum with a total width comparable with that of the whole isolated P1

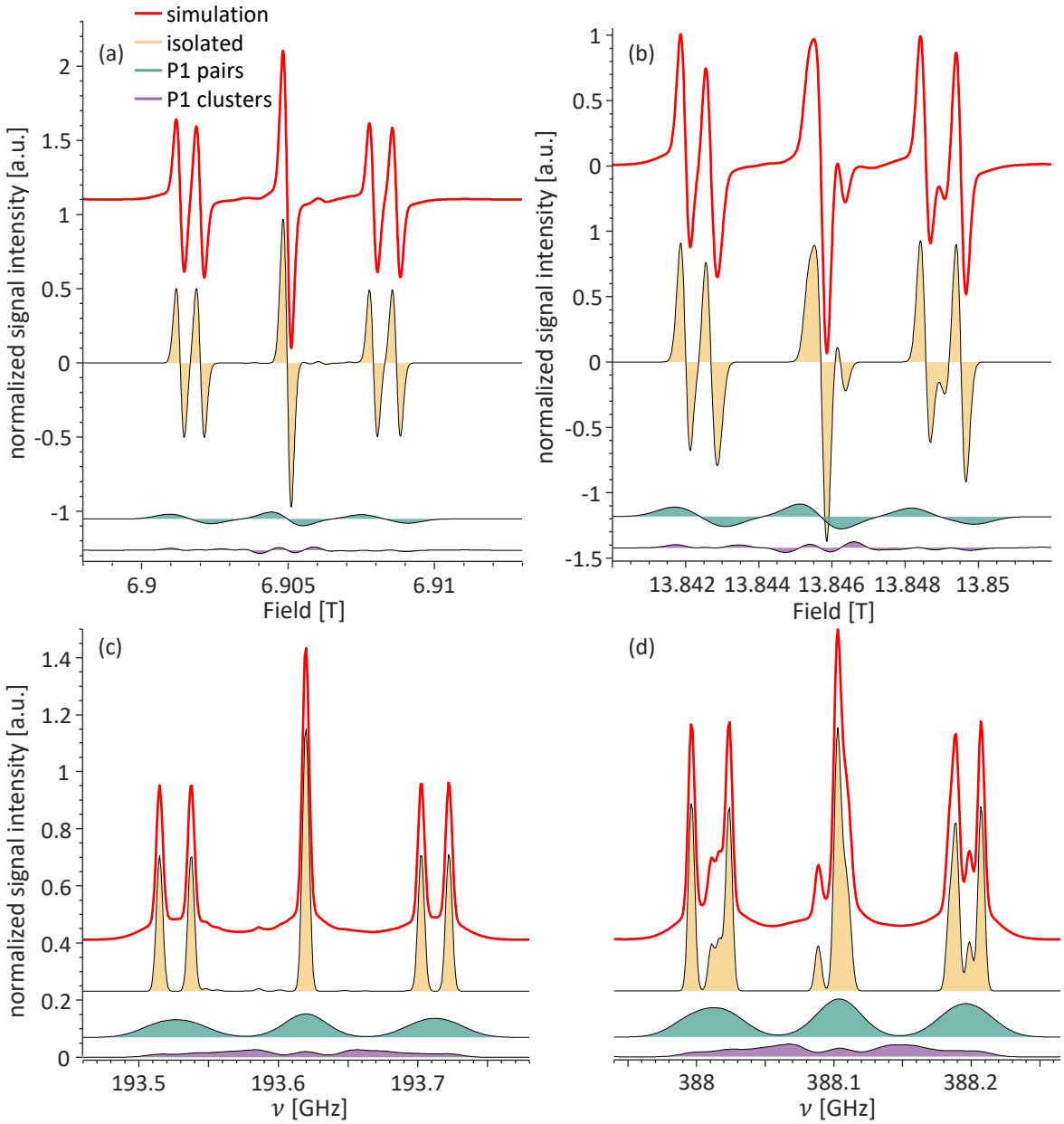

Figure S3: Decomposition of the simulated spectra, shown in Figure 6 of a single crystal HPHT diamond, into three components representing the contribution of isolated P1 centers, P1 centers pairs, and P1 center clusters. CW EPR at (a) 6.9 T and (b) 13.8 T; echo-detected pulsed EPR at (c) 6.9 T and (d) 13.8 T.

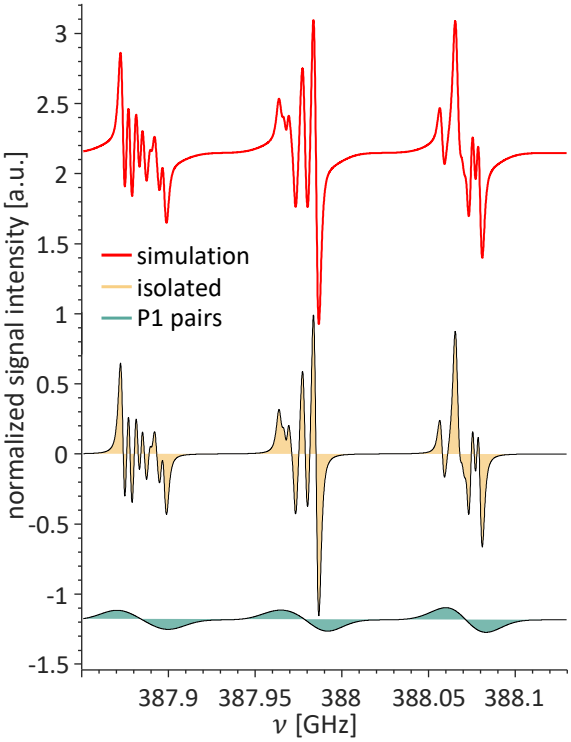

Figure S4: Decomposition of the simulated CW EPR spectra, shown in Figure 7 of a single crystal HPHT diamond at orientation B at 13.8 T, into two components representing the contribution of isolated P1 centers and P1 centers pairs.

centers spectrum. Figure S3 shows the relative contribution of each population to the simulation of the experimental spectra shown in Figure 6 in the main text. In the CW EPR spectra, the contribution of the dipolar-coupled P1 centers is not readily apparent (Figure S3a and b) and the exchange-coupled population is not observed. However, in the echo-detected EPR spectra (Figure S3c and d), the contribution of these two populations is immediately apparent, with the exchange-coupled population being the only one contributing to the signal intensity between the isolated P1 centers peaks. A description of the three populations and their interactions is detailed in a previous publication.[1]

For the simulation of the CW EPR spectrum of a single crystal diamond at Orientation B (Figure 7 in the main text and Figure S4), no contribution from the exchange-coupled P1 centers was needed. This is due to the small modulation amplitude of 0.054 mT, chosen to resolve the many lines present due to the cancellation condition for each of the four sites observed in this orientation.

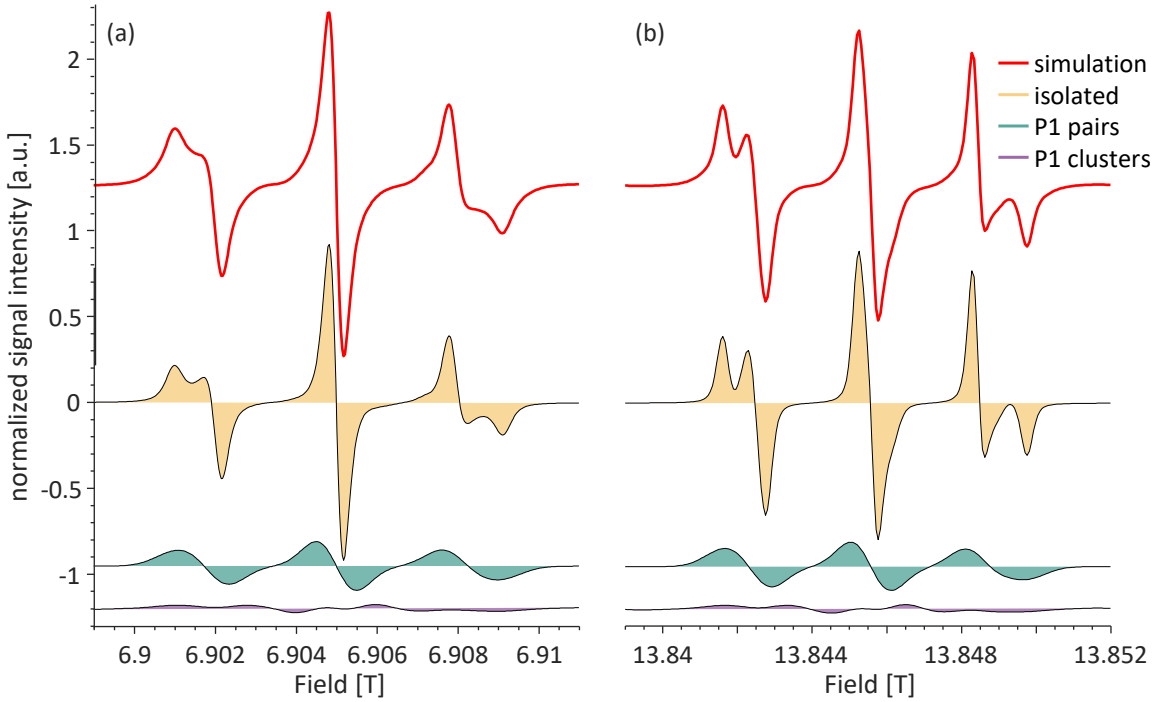

Figure S5. Decomposition of the simulated CW EPR spectra, shown in Figure 8 of a microdiamond powder, into three components representing the contribution of isolated P1 centers, P1 centers pairs, and P1 center clusters. At (a) 6.9 T and (b) 13.8 T.

The CW EPR spectra of the microdiamond powder separated into the contribution of the three P1 centers populations are shown in Figure S5. The cancellation condition effect is only evident in the EPR spectrum of the isolated P1 centers, while the large broadening in the EPR spectra of the dipolar-coupled and exchange-coupled P1 center populations obscures any subtle changes in the shape of these components between spectra acquired at 6.9 and 13.8 T.

References

(1) Nir-Arad, O.; Shlomi, D. H.; Manukovsky, N.; Laster, E.; Kaminker, I. Nitrogen Substitutions Aggregation and Clustering in Diamonds as Revealed by High-Field Electron Paramagnetic Resonance. *J. Am. Chem. Soc.* **2024**, *146* (8), 5100–5107. https://doi.org/10.1021/jacs.3c06739.